JGR Earth Surface

Supporting Information for

Modelling heat transfer for assessing the convection length in ventilated caves

Amir Sedaghatkish[1,2], Claudio Pastore[1,2], Frédéric Doumenc[3,4], Pierre-Yves Jeannin[1], Marc Luetscher[1]

[1] Swiss Institute of Speleology and Karstology (SISKA), CH-2300, La Chaux-de-Fonds, Switzerland
[2] Center for Hydrogeology and Geothermics (CHYN), University of Neuchâtel, 2000 Neuchâtel, Switzerland
[3] Université Paris-Saclay, CNRS, FAST, 91405, Orsay, France
[4] Sorbonne Université, UFR 919, 4 Place Jussieu, F-75252, Paris Cedex 05, France

Contents of this file

Introduction

Text S1 describes the method based on Fourier series to compute the time-periodic solution of the mathematical model defined in section 2.6. The numerical validation of the method is displayed in Text S2 (including Figs. **S1** to **S3**). A brief comparison between Fourier series (FS) and the resolution of the transient problem by time integration (TI) is presented in Text S3 (including Figs. **S4** to **S6**).

Text S1

The resolution by Fourier series requires a slight modification of the model defined in section 2.6. Eq. (17) resulting from the air energy balance is of order 1 in space, so that only 1 boundary condition must be imposed, the air temperature at the inlet. Since the position of the inlet changes at each flow reversal, the boundary condition has to be applied alternatively on each side of the conduct. This is possible when the problem is solved by time integration, but difficult to implement with Fourier series. This difficulty is overcome by adding a dispersion term in the air energy balance which turns to second order in space, making it possible to apply Dirichlet boundary conditions on both sides of the conduct whatever the flow direction. Eqs. (17-18) turn to:

$$\mu(\tilde{t})\, Re\, \frac{\partial \theta_a}{\partial \tilde{x}} = \left(4\frac{k_r}{k_a} Pr^{-1}\right) \tilde{\varphi}_w + Re\, Pe^{-1}\, \frac{\partial^2 \theta_a}{\partial \tilde{x}^2}\,, \tag{S1}$$

$$\theta_a(\tilde{x}=0,\tilde{t}) = \sin(2\pi\tilde{t}) \quad \text{and} \quad \theta_a(\tilde{x}=\tilde{L}_{dom},\tilde{t}) = 0. \tag{S2}$$

It is important to note that the new dispersion term in Eq. (S1) is a numerical trick with no physical sense. If the Peclet number Pe is large enough, the addition of the

dispersion term in Eq. (S1) does not significantly modify of the model output. An exception is the outlet region, where the dispersion term induces the air temperature to fit the external temperature at the end of the conduct. This change in the air temperature field takes place over a distance from the outlet of the order of Pe^{-1}, which can be arbitrarily small if Pe is large enough. The constant value $Pe = 10^5$ was set in all the simulations. We checked on a few cases that imposing $Pe = 10^6$ did not change the results.

In a second step, all the functions of time are approximated by truncated Fourier series and inserted in the mathematical model. These functions of time include:

- Two model inputs: the reduced air flowrate $\mu(\tilde{t})$ and heat transfer coefficient $\eta(\tilde{t})$.
- Two model outputs: the rock and air temperatures, respectively $\theta_w(\tilde{x}, \tilde{r}, \tilde{t})$ and $\theta_a(\tilde{x}, \tilde{t})$.

We begin with the model inputs. The exact expression of $\mu(\tilde{t})$ and $\eta(\tilde{t})$ are known *a priori* (see section 2.6). Considering that $\mu(\tilde{t})$ is an odd function of time and $\eta(\tilde{t})$ an even function of time, their approximations by truncated Fourier series read:

$$\mu(\tilde{t}) = \sum_{k=1}^{N_\mu} \mu_k \sin(2\pi k\tilde{t}) \quad \text{and} \quad \eta(\tilde{t}) = \eta_0 + \sum_{k=1}^{N_\eta} \eta_k \cos(2\pi k\tilde{t}) \,, \tag{S3}$$

where μ_k and η_k are real coefficients deduced from the exact expressions of $\mu(\tilde{t})$ and $\eta(\tilde{t})$, respectively. N_μ and N_η are the number of modes taken into account. Increasing N_μ and N_η improves the accuracy of the approximated relations (S3), but requires more computational resources.

We now focus on the model outputs. The temperatures fields in the rock $\theta_r(\tilde{x}, \tilde{r}, \tilde{t})$ and in the air $\theta_a(\tilde{x}, \tilde{r}, \tilde{t})$ are approximated by the truncated Fourier series:

$$\begin{aligned} \theta_r(\tilde{x}, \tilde{r}, \tilde{t}) &= \theta_{r,0}(\tilde{x}, \tilde{r}) + \sum_{k=1}^{N_\theta} \theta_{r,k}(\tilde{x}, \tilde{r}) \cos\left(2\pi k\tilde{t} + \varphi_{r,k}(\tilde{x}, \tilde{r})\right) \\ &= \sum_{k=-N_\theta}^{N_\theta} \Theta_{r,k}(\tilde{x}, \tilde{r}) \exp(2\pi j k\tilde{t}) \,, \end{aligned} \tag{S4}$$

$$\begin{aligned} \theta_a(\tilde{x}, \tilde{t}) &= \theta_{a,0}(\tilde{x}) + \sum_{k=1}^{N_\theta} \theta_{a,k}(\tilde{x}) \cos\left(2\pi k\tilde{t} + \varphi_{a,k}(\tilde{x})\right) \\ &= \sum_{k=-N_\theta}^{N_\theta} \Theta_{a,k}(\tilde{x}) \exp(2\pi j k\tilde{t}) \,, \end{aligned} \tag{S5}$$

where the same number of modes N_θ is considered for the rock and air temperatures. The complex coefficients $\Theta_{r,k}$ are such that $\Theta_{r,-k}$ is the conjugate of $\Theta_{r,k}$. They are

related to the real amplitudes ($\theta_{r,k}$ and $\theta_{a,k}$) and phase shifts ($\varphi_{r,k}$ and $\varphi_{a,k}$) through the standard relations:

$$\theta_{r,0} = \Theta_{r,0} \quad \text{and} \quad \theta_{a,0} = \Theta_{a,0}\,, \tag{S6}$$

$$\theta_{r,k} = 2\sqrt{\Theta_{r,k}\Theta_{r,-k}} \quad \text{and} \quad \theta_{a,k} = 2\sqrt{\Theta_{a,k}\Theta_{a,-k}} \quad \text{for} \quad k>0\,, \tag{S7}$$

$$\tan\varphi_{r,k} = -\frac{j\,(\Theta_{r,k}-\Theta_{r,-k})}{\Theta_{r,k}+\Theta_{r,-k}} \quad \text{and} \quad \tan\varphi_{a,k} = -\frac{j\,(\Theta_{a,k}-\Theta_{a,-k})}{\Theta_{a,k}+\Theta_{a,-k}} \quad \text{for} \quad k>0\,. \tag{S8}$$

Injecting Eqs. (S3-S5) in the mathematical model of section 2.6 yields the equations:

$$\frac{Re}{2j}\sum_{m=1,3...}^{N_\mu}\mu_m\Big(\frac{\mathrm{d}\Theta_{a,k-m}}{\mathrm{d}\tilde{x}}-\frac{\mathrm{d}\Theta_{a,k+m}}{\mathrm{d}\tilde{x}}\Big) = \left(4\frac{k_r}{k_a}Pr^{-1}\right)\tilde{\Phi}_{w,k} + RePe^{-1}\,\frac{\mathrm{d}^2\Theta_{a,k}}{\mathrm{d}\tilde{x}^2}\,, \tag{S9}$$

$$\Theta_{a,k}(\tilde{x}=0) = \frac{1}{2j} \quad \text{for } k=1, \quad \Theta_{a,k}(\tilde{x}=0) = 0 \quad \text{for } k\neq 1\,, \tag{S10}$$

$$\Theta_{a,k}(\tilde{x}=\tilde{L}_{dom}) = 0, \tag{S11}$$

$$2\pi jk\,\Theta_{r,k} = \frac{1}{\tilde{r}}\frac{\partial}{\partial\tilde{r}}\left(\tilde{r}\frac{\partial\Theta_{r,k}}{\partial\tilde{r}}\right) + \frac{\partial^2\Theta_{r,k}}{\partial\tilde{x}^2}\,, \tag{S12}$$

$$\Theta_{r,k}(0,\tilde{r}) = \frac{1}{2j} \quad \text{for } k=1, \quad \Theta_{r,k}(0,\tilde{r}) = 0 \quad \text{for } k\neq 1\,, \tag{S13}$$

$$\frac{\partial\Theta_{r,k}}{\partial\tilde{x}}(\tilde{x}=\tilde{L}_{dom},\tilde{r}) = 0 \quad \text{and} \quad \frac{\partial\Theta_{r,k}}{\partial\tilde{r}}(\tilde{x},\tilde{r}=\tilde{R}_{dom}) = 0\,, \tag{S14}$$

$$\begin{aligned}\text{Case A}: \ \tilde{\Phi}_{w,k} &= \frac{\partial\Theta_{r,k}}{\partial\tilde{r}}(\tilde{x},\tilde{R}) \\ &= Bi\sum_{n=0,2,...}^{N_\eta}\frac{\eta_n}{2}\left[\Theta_{r,k-n}(x,\tilde{R}) - \Theta_{a,k-n}(\tilde{x}) + \Theta_{r,k+n}(\tilde{x},\tilde{R}) - \Theta_{a,k+n}(\tilde{x})\right]\,,\end{aligned} \tag{S15}$$

$$\text{Case B}: \ \tilde{\Phi}_{w,k} = \frac{\partial\Theta_{r,k}}{\partial\tilde{r}}(\tilde{x},\tilde{R}) \quad \text{and} \quad \Theta_{a,k}(\tilde{x}) = \Theta_{r,k}(\tilde{x})\,, \tag{S16}$$

where $j=\sqrt{-1}$ and k is an integer varying from 0 to N_θ. Eqs. (S9) and (S12) thus define a set of $2(N_\theta+1)$ coupled partial differential equations (PDE) with boundary conditions (S10-S11,S13-S16). This set of PDE, which does not include the time variable $\tilde{t}$, is solved numerically by finite elements (Galerkin method with quadratic Lagrangian elements, Comsol Multiphysics software). The resolution yields the complex coefficients $\Theta_{r,k}(\tilde{x},\tilde{r})$ and $\Theta_{a,k}(\tilde{x})$. The real amplitudes and phase shifts are deduced from relations (S7-S8) and the temperatures as a function of time from relations (S4-S5).

Text S2

The choice of N_μ, N_η and N_θ results from a compromise between the accuracy of the results on one hand, the difficulty of the implementation and the available computational resources on the other hand. The sensitivity of the simulation results to N_θ, N_μ and N_η is investigated below for case A with $\tilde{R} = 0.2$ and $Re = 7.2 \times 10^5$.

We first set $N_\eta = 0$ and $N_\mu = 1$ and we investigate the effect of N_θ. Figs. **S1** display the effect of N_θ on the time series of the wall temperature at $\tilde{x} = 10$ and $\tilde{x} = 100$. The general shape of the curve is little modified for $N_\theta \geq 6$, but the description of the rapid oscillations around $\tilde{t} \simeq 0.05$ and $\tilde{t} \simeq 0.45$ requires a larger number of modes. The same approach is used to investigate the effect of N_η and N_μ. Figs. **S2** show that these parameters has little effect on the results for the selected configuration. In all the simulations, we imposed $N_\theta = 18$, $N_\eta = 6$ and $N_\mu = 7$ which happened to be a reasonable compromise between accuracy and complexity. We checked on a few configurations that increasing the number of modes above the selected values did not significantly changed the results.

In order to confirm its validity, the numerical solution based on Fourier series was compared with the solution obtained by time integration (Galerkin method with quadratic Lagrangian elements, time discretization using implicit Backward Differentiation Formula, Comsol Multiphysics software). The TI simulation was done over 28 cycles (i.e., from time $\tilde{t} = 0$ to $\tilde{t} = 28$) taking as the initial condition the solution obtained from Fourier series at $\tilde{t} = 0$. The comparison between TI (last cycle, from time $\tilde{t} = 27$ to 28) and FS is displayed in Fig. **S3**. Small discrepancies are observed during the rapid oscillations around times $t \simeq 0.05$ and $t \simeq 0.45$ for $\tilde{x} = 10$ and $\tilde{x} = 100$, but the overall agreement is excellent.

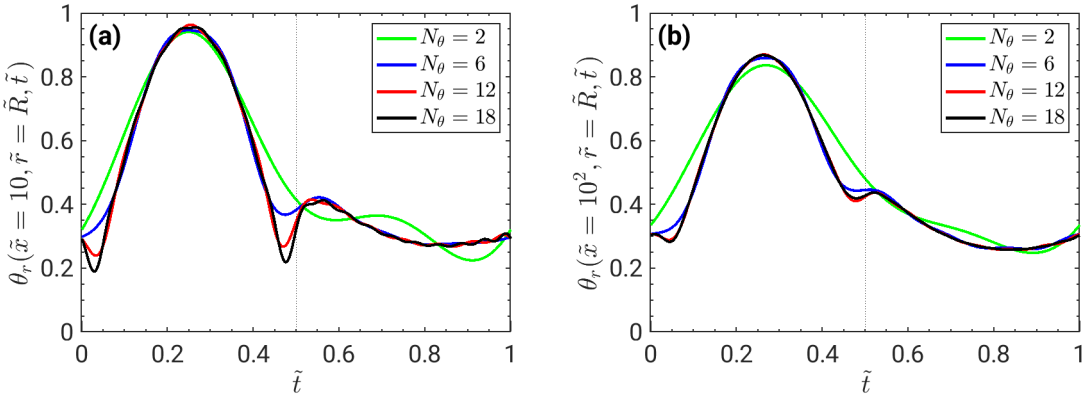

Figure S1. Time evolution of the wall temperature at $\tilde{x} = 10$ (a) and $\tilde{x} = 100$ (b) for $N_\eta = 0$, $N_\mu = 1$ and different values of N_θ. Case A with $\tilde{R} = 0.2$ and $Re = 7.2 \times 10^5$.

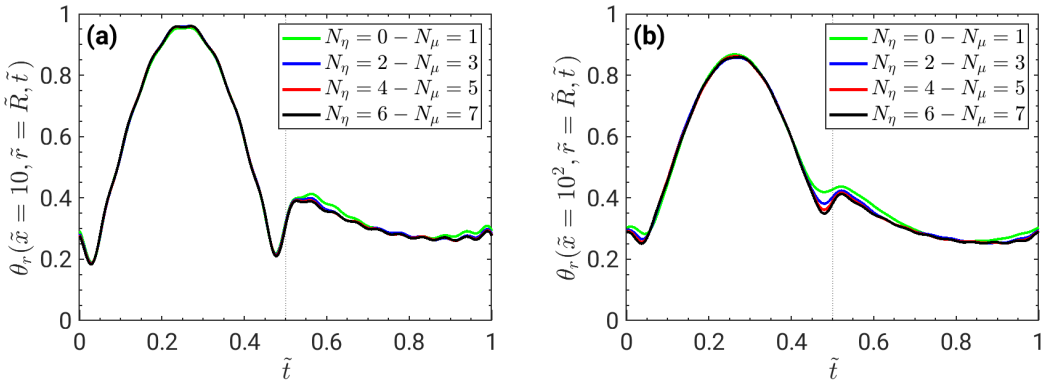

Figure S2. Time evolution of the wall temperature at $\tilde{x} = 10$ (a) and $\tilde{x} = 100$ (b) for $N_\theta = 18$ and different values of N_η and N_μ. Case A with $\tilde{R} = 0.2$ and $Re = 7.2 \times 10^5$.

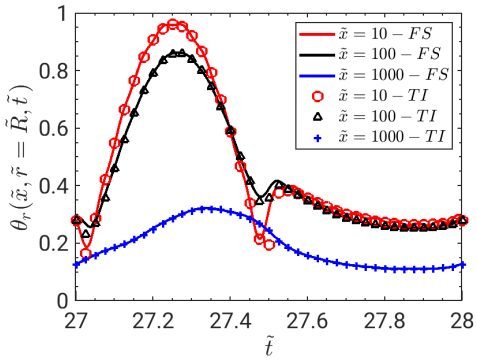

Figure S3. Time evolution of the conduit wall temperature calculated using Fourier series (FS) or time integration (TI), at different distances from the entrance $\tilde{x}$. FS solution at $\tilde{t} = 0$ used as the initial condition of TI simulation. Case A with $\tilde{R} = 0.2$ and $Re = 7.2 \times 10^5$.

Text S3

A standard approach, not used in this study, would consist in solving the time-dependent problem by TI starting from an arbitrary initial condition (e.g., $\theta_r(\tilde{x}, \tilde{r}, \tilde{t} = 0) = \theta_a(\tilde{x}, \tilde{t} = 0) = 0$). The time-dependent solution converges to the periodic regime at infinite time. A good approximation can thus be obtained if the simulated time is long enough. Figures (**S4-S6**) display the parameters defined in Section 4 calculated from TI as a function of time or FS, for case A with $\tilde{R} = 0.189$ and $Re = 1.8 \times 10^5$. With the exception of $\tilde{W}_1$, TI results converge slowly to the periodic regime. Taking FS as a reference, TI yields errors at time $\tilde{t} = 50$ in the range from 10% to 30% for $\bar{\theta}_w$, $\Delta\theta_w$, $\tilde{L}_0$ and $\tilde{L}_1$. These errors are acceptable if rough estimates are required. In contrast, TI underestimates $\tilde{W}_0$ by an order of magnitude. To get a correct estimate of this parameter and improve the accuracy of others, TI would require to simulate a time of the order of the diffusion time $\tilde{W}_0^2 \simeq 64^2 \sim 4 \times 10^3$, i.e. thousands of years. Such simulations would require computational times hardly compatible with current computer resources.

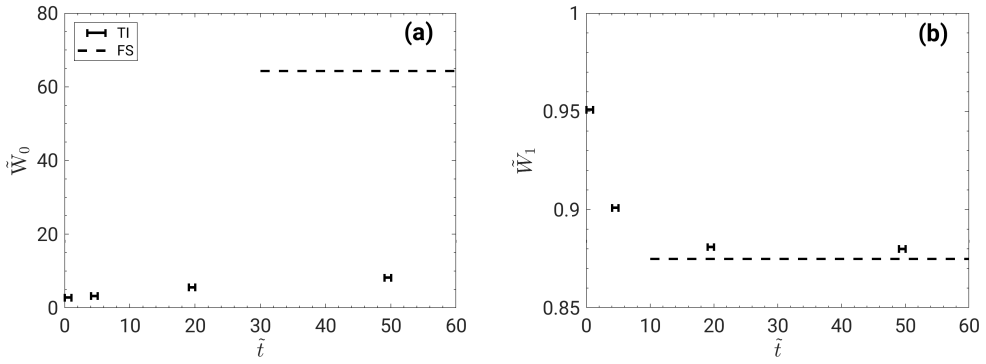

Figure S4. $\tilde{W}_0$ (a) and $\tilde{W}_1$ (b) estimated from Fourier series (FS) or time integration (TI). Initial conditions in TI simulations set to zero. Case A with $\tilde{R} = 0.189$ and $Re = 1.8 \times 10^5$.

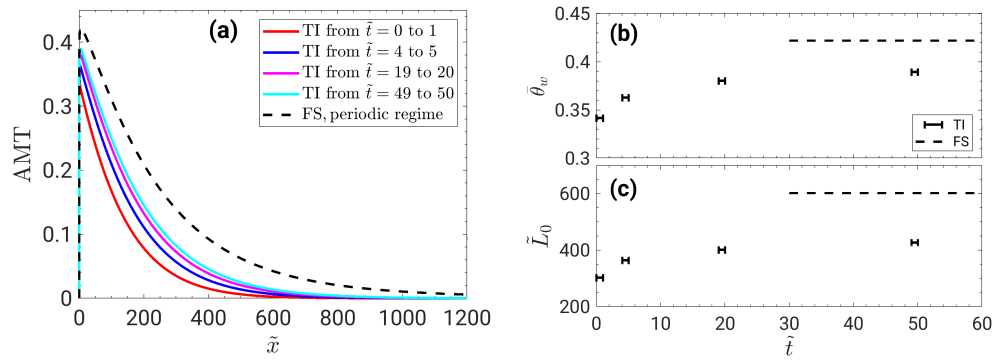

Figure S5. AMT of the conduct wall (a), $\bar{\theta}_w$ (b) and $\tilde{L}_0$ (c) estimated from Fourier series (FS) or time integration (TI). Initial conditions in TI simulations set to zero. Case A with $\tilde{R} = 0.189$ and $Re = 1.8 \times 10^5$.

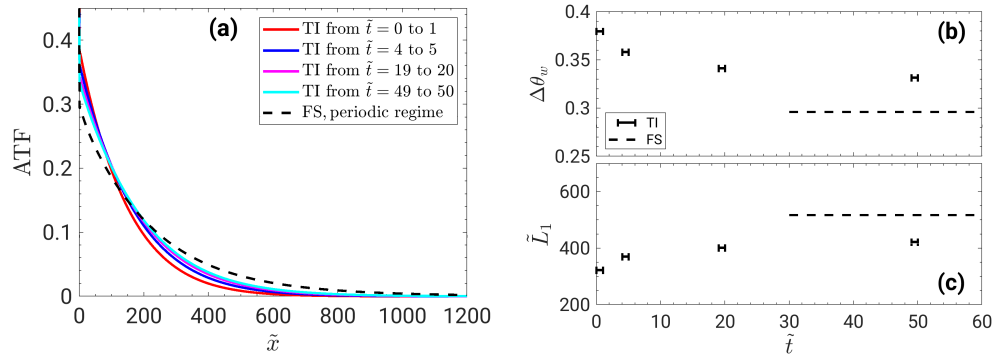

Figure S6. ATF of the conduct wall (a), $\Delta\theta_w$ (b) and $\tilde{L}_1$ (c) estimated from Fourier series (FS) or time integration (TI). Initial conditions in TI simulations set to zero. Case A with $\tilde{R} = 0.189$ and $Re = 1.8 \times 10^5$.